Control and Analysis of a Modular Bridge for Battery Cell Voltage Balancing

Atrin Tavakoli, *Student Member, IEEE*, S. Ali Khajehoddin, *Senior Member, IEEE*, and John Salmon, *Member, IEEE*

***Abstract*—A new distributed control scheme and charge flow analysis is presented for voltage balancing of series connected battery cells using nondissipative modular power electronics. Each modular bridge is connected across two battery cells using a high frequency transformer and an asymmetrical half-bridge. This results in using one switch and one diode per battery cell. Intrabridge charge transfer equalizes the voltage of two battery cells within a module using coupled transformer windings. Each modular bridge is connected to adjacent bridges by connecting transformer windings within each module. This allows interbridge charge transfer and the balancing of pairs of battery cells, both within adjacent bridge modules and modules more removed. The proposed controller uses a distributed control strategy whereby the control of each modular bridge monitors its own battery cell voltages and also those of adjacent bridges, thus reducing the number of feedback sensors. Detailed analysis is presented that quantifies the flow of charge between a number of series connected battery cells (N battery cells). A per-unit design methodology is used to illustrate the system charge flow characteristics. Simulations, design guidelines and experimental results are presented to validate the proposed method.**

***Index Terms*—Battery, modular circuit, supercaps, two-switch flyback, voltage balancing.**

I. Introduction

SERIES-CONNECTED battery cells are increasingly being used in high dc voltage applications, such as hybrid electric vehicles and energy storage centers in many industrial and utility applications. Series-connected battery cell topologies are often charged and discharged using the same series current. Therefore, a small difference in battery cells capacitance may lead to overcharging and over discharging in battery cells. Some battery cells, such as Li-ion, are sensitive to overcharging/overdischarging and may expose irreversible battery cell damage and reduced lifetime expectancies [1]–[3]. To prevent these issues, the charge equalization or voltage balancing techniques can be used.

Battery charge equalization or voltage balancing techniques can be categorized into dissipative [4]–[6] and nondissipative [7]–[26] types. The nondissipative circuits improve the efficiency of the balancing mechanism and can be categorized into: charge shuttling, charge shunting [7]–[9], and dc/dc converter equalization techniques [10]–[26]. Charge shunting and charge shuttling use switched capacitors to transfer charge between battery cells [7], [8]. Although these methods normally require complex centralized control systems, their implementations are relatively straightforward.

In dc/dc converter based approaches, normally a high number of power switches as well as a central battery management system (BMS) are utilized. For example in [10], the state of charge (SOC) balancing is performed using a dual active bridge between each battery and a low voltage bus. Such methods are effective, accurate but due to high number of switches and sensors the overall system becomes expensive. The system cost can be slightly reduced by lowering the number of switches [11] or lowering the switch voltage stress [12], [13]. In most of the dc/dc converter based approach, a transformer or an inductor is used to control the charge transfer [14], [15]. In [16], a multiwinding transformer is used to couple battery cells and in [17] a multiwinding transformer along with a resonant circuit is used to couple all the battery cells and reduce the stress on the switches. Although these methods transfer charge rapidly between nonneighbor battery cells, due to the physical limitation of a multiwinding transformer, their applications are limited to cases when a small number of battery cells are used. If an inductor is used rather than a transformer, the charge transfer between neighboring battery cells becomes feasible with a smaller circuit size and a lower weight but at a slower speed of charge equalization [18]. Methods where transformers or inductors are used, normally need a voltage sensor per a battery cell resulting in a high number of sensors and higher cost. In [12], [13], [19], [23], and [24], a resonant circuit is used to transfer charge between battery cells to reduce the energy losses and emi/rfi emissions. Some methods, such as [18] use inductors to transfer charge to the neighboring bridges resulting in a pretty slow charge transfer as it happens only between neighboring bridges. Specifically, when battery cells with low voltage are not close to battery cells with higher voltage, these methods are slow. Other topologies are also proposed to improve the speed of charge equalization [21], [22]; however, generally, such topologies are not modular.

A new controller for a modular two-switch flyback battery cell voltage balancing circuit is presented. A single modular bridge cell (BC) consists of an asymmetrical half bridge with

Manuscript received July 23, 2017; revised October 27, 2017 and December 21, 2017; accepted January 11, 2018. Date of publication January 26, 2018; date of current version August 7, 2018. Recommended for publication by Associate Editor M. Ferdowsi. *(Corresponding author: Atrin Tavakoli.)*

The authors are with the School of Electrical and Computer Engineering, University of Alberta, Edmonton, AB T6G 2R3, Canada (e-mail: atrin@ualberta.ca; khajeddin@ieee.org; john.salmon@ualberta.ca).

Color versions of one or more of the figures in this paper are available online at http://ieeexplore.ieee.org.

Digital Object Identifier 10.1109/TPEL.2018.2798636

TABLE I
COMPARING DIFFERENT METHODS FOR A SYSTEM WITH $2n$ BATTERY CELLS

Feature \ Method	[10]	[12]	[13]	[16]	[17]	[18]	[24]	PROPOSED METHOD
Modularity	✔	✘	✔	✔	✘	✔	✔	✔
Non-neighbor Batteries Charge Transfer	✔	✔	✘	✔	✔	✘	✔	✔
Supports Unlimited Number of Batteries	✔	✘	✔	✔	✘	✔	✔	✔
Charge Transfer Between More than Two Battery Cells in Each Cycle	✔	✔	✘	✘	✘	✘	✔	✔
Number of Switches / Diodes	$16n/0$	$2/4n+2$	$2n/0$	$2n/2n$	$4n/2n$	$4n-2/0$	$4n+2/8n$	$2n/2n$
Number of Sensors	$4n$	0	$2n$	$2n$	$4n$	$2n$	$2n$	n
Central/Distributed Controller	Dist.	Dist.	Cent.	Cent.	Cent.	Cent.	Dist.	Dist.
Complexity	Simple	Simple	Simple	Complex	Complex	Simple	Complex	Simple

a four winding transformer connected to two battery cells. The BC topology is modular with a low switch count per battery cell. Each BC balances its own two battery cells using magnetically coupled windings connected to the centre tap of the two battery cells. Charge transfer to and from battery cell pairs in adjacent BCs is decided locally within each bridge by monitoring the dc voltages of the battery cells connected to adjacent bridges. Therefore, the system requires only one voltage sensor per battery cell pair. This 'distributed" controller is based on local data without requiring a BMS or a central controller. Faster voltage balancing is achieved at a high efficiency using no current sensors and fewer voltage sensors when compared with the conventional methods.

The proposed distributed control improves upon previously published controllers using the same topology [20], [25], [26]. The controller has a much faster battery cell charge equalization than was obtained in [20]. The controller also uses a more simplified switching pattern than that is presented in [25] and [26]: two switching patterns per switching cycle are used rather than three. The proposed control is demonstrated to transfer charge among neighboring BCs in one switching cycle, but can also transfer charge among all bridges. The structure and operation of the modular BC is examined to derive a new simplified system circuit model that contains a series of $2n$ connected battery cells with n BCs. This simplified model uses per-unit design parameters to provide a detailed charge flow analysis, select appropriate circuit inductance and to place limits placed on the controller switching periods. A maximum battery cell voltage deviation is assumed in the design procedures together with the following design guidelines.

1) A maximum component peak current.
2) A maximum switching frequency where all circuit currents reach zero at the end of each switching cycle.
3) The controller maximizes the charge transfer rate.

Finally, Table I compares the modular circuit and its proposed controller with previously published work.

II. CIRCUIT TOPOLOGY

A single bridge cell, or in the shorter form bridge or BC, consists of a asymmetric half-bridge, two series connected battery cells, and a toroidal transformer with four windings, see Fig. 1: w_1, $w_{1'}$, w_2, and $w_{2'}$. The magnetizing inductance

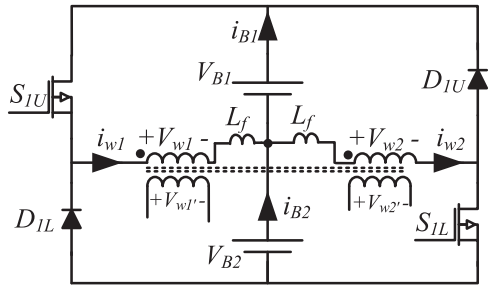

Fig. 1. Single BC connected to two battery cells using an asymmetric half-bridge and a four-winding toroidal transformer and the added inductor.

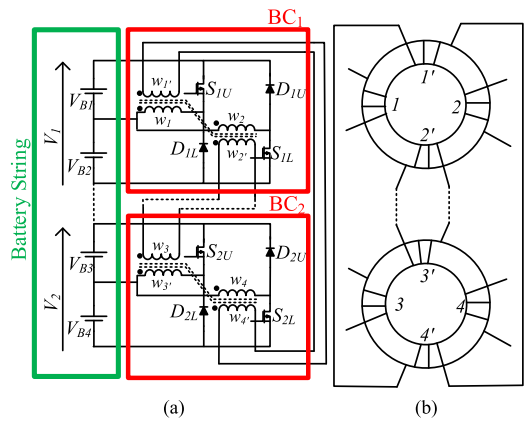

Fig. 2. Connection of two BCs to four battery cells: (a) circuit and (b) four-winding toroidal transformer.

associated with the transformer windings w_1 and w_2 places a limit on the peak current that is common to both windings during the switch on time. Conversely, L_f controls the difference between the winding currents that can also produce large peak winding currents: L_f is necessary due to the very low leakage inductance of the transformer windings (typical 0.1%). The transformer windings $w_{1'}$ and $w_{2'}$ is used to couple one bridge with its neighboring bridges, making the topology modular: see Fig. 1 for a one-bridge system, Fig. 2 for two bridges, Fig. 3(a) for a multi bridge system.

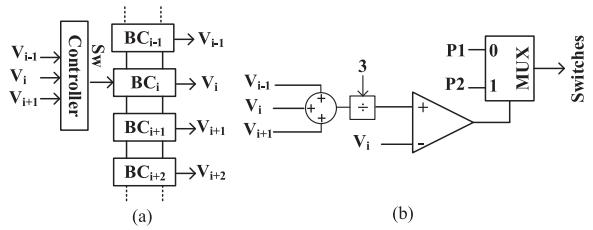

Fig. 3. Controller for a series of connected BCs: (a) cells with their interbridge transformer winding connections and bridge dc voltages Vi, V_{i-1} etc. and (b) switching logic for BC$_i$ using two switching patterns, $P1$ and $P2$ (see Fig. 5).

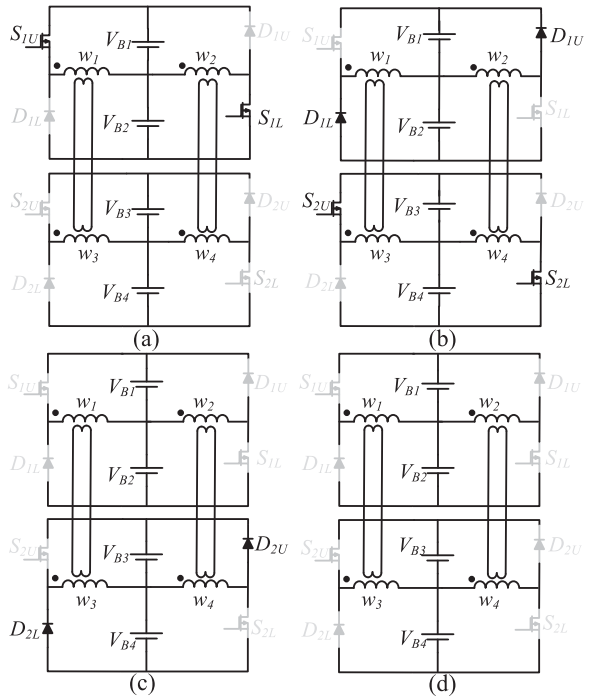

Fig. 4. Switching states for two bridges when $V_{B1} + V_{B2} > V_{B3} + V_{B4}$ or in other words $V_1 > V_2$: (a) State 1, (b) State 2, (c) State 3, and (d) State 4.

III. Principle of Operation and Control: Two-Switch Flyback

The distributed controller chooses the switching pattern of each bridge by monitoring the dc battery cell voltages in adjacent bridges, see Fig. 3. The dc voltage V_i of BC$_i$ (sum of its two battery cell voltages) is compared with the average of the adjacent bridge voltages and its own: $[(V_{i-1} + V_i + V_{i+1})/3]$. If V_i is the largest voltage, BC$_i$ chooses the switching pattern "P1." If BC$_i$ does not have the largest, it chooses the switching pattern "P2," see Figs. 4 and 5 for "P1" and "P2."

The bridge switching patterns for two BCs, Fig. 2, are illustrated in Fig. 4. The battery cell voltages in BC$_1$ are assumed to be $V_{B1} > V_{B2}$. BC$_1$ is assumed to have the higher voltage ($V_1 > V_2$) and chooses the switching pattern $P1$, BC$_2$ having the lowest voltage chooses $P2$:

State 1 [0-x_1]:

At the beginning of a switching cycle, the switches in BC$_1$ are turned ON and kept OFFin BC$_2$ [see Fig. 4(a)]. Currents increase through windings w_1 and w_2, i_{w1} and i_{w1}, respectively,

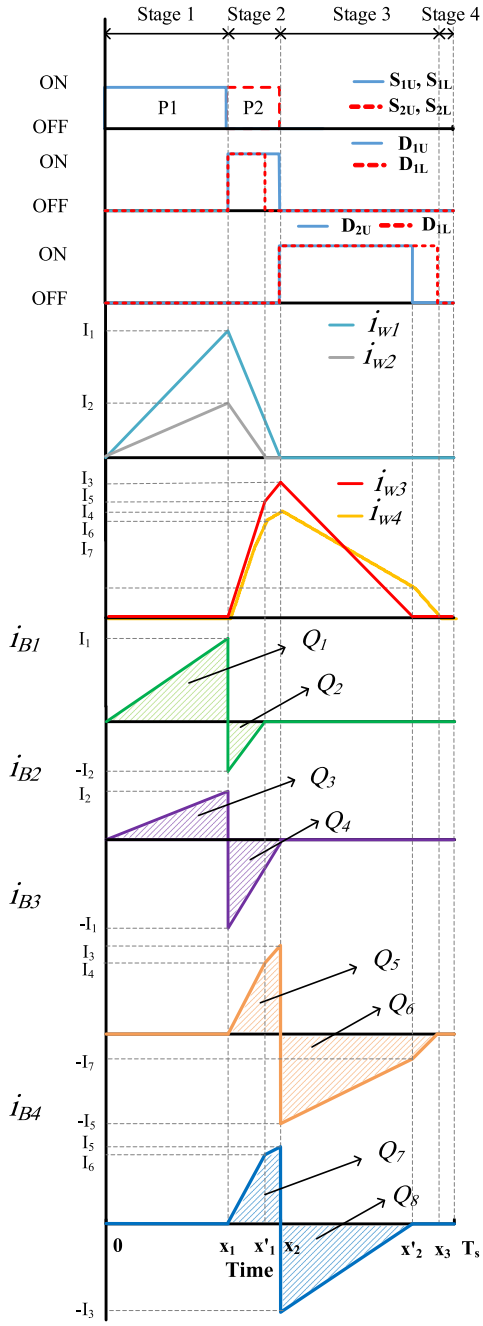

Fig. 5. Current waveforms of the two-bridge system shown in Fig. 2.

increasing proportional to V_{B1} and V_{B2}, see Fig. 1 for the currents directions and Fig. 5 for the currents diagrams. Since $V_{B1} > V_{B2}$, i_{w1} increases more rapidly and reaches a higher value ($I_1 > I_2$). At the end of this switching state, the switches in BC$_1$ are turned OFF.

State 2 [x_1-x_2]:

The diodes in BC$_1$ turn ON to create a path for the winding w_1, w_2 currents [see Fig. 4(b)]. The switches in BC$_2$ are turned ON. Some of the stored energy in the magnetic core will be transferred from BC$_1$ to BC$_2$, hence from V_1 to V_2, respectively, representing intrabridge charge transfer.

Since $I_1 > I_2$ and $V_{B1} > V_{B2}$, i_{w2} reaches zero before i_{w1} [see Fig. 5]. This results in charge being transferred from V_{B1}

to V_{B2}, intrabridge charge transfer, see i_{B1} and i_{B2} in Fig. 5. However, significant charge is also removed from BC_1 and transferred to BC_2: the currents increasing in w_3 and w_4, representing interbridge charge transfer.

The winding voltages V_{w1} and V_{w2} are increased above V_1 by the on-state diode voltages in BC_1, and i_{w2} drops down to zero rapidly as a result. After this point, the winding voltage drop in BC_2 drops, resulting in the current ramping rate in BC_2 to drop, see i_{w3} in Fig. 5. This state continues until the BC_2 switches are turned OFF.

State 3 [x_2-x_3]:

All switches are turned OFFand only the diodes in the second bridge are ON [see Fig. 4(c)]. This represents the transfer of energy from BC_1 and BC_2, respectively. This state continues until the currents of through all the transformer windings return to zero. Similar to the previous mode, when one of the currents reaches zero the ramping rate of the other bridges change.

State 4 [x_3-T_s]:

All switches and diodes are OFFuntil the next state starts [see Fig. 4(d)].

In Fig. 5, the areas under the current waveforms represent the exchange charge. Examination of i_{B1}, i_{B2} for instance, represent exchanged charge of battery cells in BC_1. For example, the exchanged charge of battery cell 2 in Fig. 5 equals to

$$Q_{B2} = \int_0^{T_s} i_{B_2}(t)dt = \int_0^{t_1} i_{w_2}(t)dt - \int_{t_1}^{t_2} i_{w_1}(t)dt = \frac{I_2 \times t_1}{2} - \frac{I_1 \times (t_2 - t_1)}{2} = Q_3 - Q_4. \quad (1)$$

Comparing $Q_{B1} = Q_1 - Q_2$ and Q_{B2}, in Fig. 5, it can be concluded that $Q_{B1} > Q_{B2}$, thus, battery cell 1 transfers more charges compare to battery cell 2. Similarly, it can be concluded that battery cell 3 and battery cell 4 absorb charge.

IV. Circuit Analysis and Design Constraints

Circuit analysis is presented for a system containing a series of $2n$ connected battery cells with n BCs. This analysis is used to design the circuit inductances and the controller switching periods. Given that the system is designed for a maximum allowable battery cell voltage deviation, this analysis also assumes the following design guidelines:

1) a maximum peak current for the components;
2) a maximum switching frequency where all circuit currents reach zero at the end of each switching cycle;
3) the controller is maximizing the charge transfer rate.

Since inductance values can have a large variation, the effects of these variations on charge transfer charge are examined, including a charge back flow phenomenon. Lastly, a step-by-step design procedure is given, resulting in specifying the desirable size of the system inductances and switching time periods in a switching cycle.

A. Analysis

An equivalent circuit for an $2n$ battery cell system (n BCs) can be constructed together with a system matrix representation. The latter can be used to predict the system currents and switching periods, see Fig. 5, over a switching cycle. The circuit for the BC_1 in Fig. 4(a) is redrawn in Fig. 6(a), and represented in with a general equivalent circuit in Fig. 6(b) that has the circuit voltage waveforms shown in Fig. 6(c).

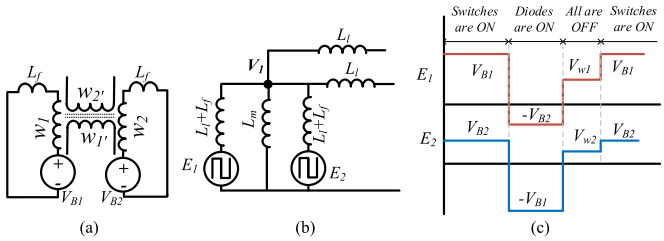

Fig. 6. BC equivalent circuit of Fig. 1: (a) rearranged representation, (b) general equivalent circuit, and (c) voltage waveform of E_1 and E_2 (L_m: magnetizing inductance for two windings, L_l: leakage inductance for two windings, L_f added series inductance).

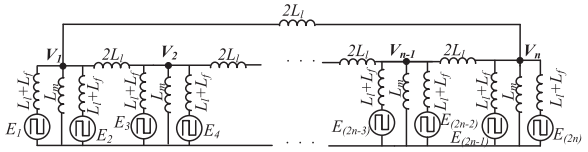

Fig. 7. Equivalent circuit of a system with "n" bridges and "$2n$" battery cells.

The general equivalent circuit for a BC in Fig. 6(c), can be extended to a system containing "n" BCs and "$2n$" battery cells, as shown in Fig. 7 and with the matrix representation given in (2)

$$\begin{bmatrix} L_{1,1} & L_{1,2} & L_{1,3} & \dots & \dots & L_{1,2n} \\ L_{2,1} & L_{2,2} & L_{2,3} & \dots & \dots & L_{2,2n} \\ \dots & \dots & \dots & \dots & \dots & \dots \\ \dots & \dots & \dots & \dots & \dots & \dots \\ \dots & \dots & \dots & \dots & \dots & \dots \\ L_{2n,1} & L_{2n,2} & L_{2n,3} & \dots & \dots & L_{2n,2n} \end{bmatrix}^{-1} \times \begin{bmatrix} v_{w1} \\ v_{w2} \\ \dots \\ \dots \\ \dots \\ v_{w(2n)} \end{bmatrix} = \frac{d}{dt} \begin{bmatrix} i_{w1} \\ i_{w2} \\ \dots \\ \dots \\ \dots \\ i_{w(2n)} \end{bmatrix} \rightarrow \begin{cases} [L_{pq}]^{-1} \times [v_{w,p}] = [a_{pq}] \times [v_{w,p}] \\ [a_{pq}] \times [v_{w,p}] = \frac{d}{dt}[i_{w,p}] \end{cases}, 1 < p, q < 2n \quad (2)$$

L_{ii}—self-inductance; L_{ij}—mutual inductance between winding i and j; V_w, i_{wi} voltage and current of the ith winding. The "a" matrix is the inverse of "L" matrix. All the coupled inductors are assumed to be the same and the circuit is assumed symmetrical, therefore, self-inductances are the same: $L_{ii} = L_{jj}$ and $L_{ij} = L_{ji}$, and defined

$$L_{\text{ii}} = \frac{L_l + L_f}{\frac{-Y^{-1}(1,1)}{(L_l + L_f)} + 1} = \frac{(L_l + L_f)^2}{-Y^{-1}(1,1) + L_l + L_f}$$

$$L_{\text{ij}} = L_{\text{ji}} = L_{\text{ii}} \frac{Y^{-1}(j,1)}{(L_l + L_f)} = \frac{(L_l + L_f) \times Y^{-1}(j,1)}{-Y^{-1}(1,1) + L_l + L_f}. \quad (3)$$

The Y matrix can be found by applying KCL on Fig. 7, see (4) shown at the bottom of this page.

With the components of matrix L determined, (2), an expression for all the system currents for every switching condition can be obtained. For example, in state 1, Fig. 4(a), the ramping rate of i_{w1} can be calculated as follows:

$$\frac{d}{dt}i_{w1}(t) = V_{B1} \times a_{11} + V_{B2} \times a_{12} + V_{w3} \times a_{13} + V_{w4} \times a_{14} \tag{5}$$

where a_{ij} is the element of ith row and jth column of matrix "a". In (2), V_{wi} is the voltage of the ith winding and can be calculated as follows:

$$V_{wi} = \frac{V_{B1} + V_{B2}}{L_{11} + L_{12}} \times L_{1i}. \tag{6}$$

More generally, for n BCs and $2n$ battery cells, consider when

1) the switches in bridges 1 to "k" are ON;
2) the diodes of bridges "$k+1$" to "m" are ON;
3) the switches and diodes of bridges "$m+1$" to "n" are OFF.

Accordingly, the system equation can be written

$$[a_{pq}] \times \begin{bmatrix} V_{B1} \\ \dots \\ V_{B(2k)} \\ -V_{B(2k+2)} \\ \dots \\ -V_{B(2m-1)} \\ v_{w(2m+1)} \\ \dots \\ v_{w(2n)} \end{bmatrix} = \frac{d}{dt} \begin{bmatrix} i_{w1} \\ \dots \\ i_{w(2k)} \\ i_{w(2k+1)} \\ \dots \\ i_{w(2m)} \\ 0 \\ \dots \\ 0 \end{bmatrix}. \tag{7}$$

The $2n$ unknown variables in (7) are currents $(i_{w1}, \dots, i_{w(2m)})$ of the bridges whose switches or diodes are ON, and the inductors voltage $(v_{w(2m+1)}, \dots, v_{w(2n)})$ of bridges whose switches and diodes are OFF. As there are $2n$ equations, a unique solution can always be found.

B. Design

Assuming a maximum and minimum allowable battery cell voltage, the design constraints are as follows:

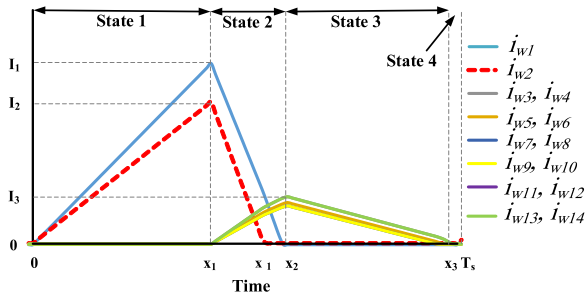

Fig. 8. Current waveforms of a seven-bridges system under case1.

1) The system maximum peak current defined ($I_{\max}$).
2) A fixed switching frequency (f_s) is assumed where all system currents reach zero at the end of the cycle.
3) The controller is designed to maximize charge transfer rate.

To make sure these constraints and requirements are met in all the conditions, two extreme-case scenarios are considered:

Case Scenario 1: Battery cell 1 has the highest possible voltage and the others have the lowest possible voltage.

Case Scenario 2: Battery cell 1 has the lowest possible voltage and the others have the highest possible voltage.

1) Case Scenario 1: This case results in bridge 1 choosing switching pattern $P1$ and rest choose $P2$, see Figs. 5 and 8. During the first switching state, the switches BC_1 are turned ON and i_{w1} and i_{w2} increase. Since battery cell 1 has the highest voltage, i_{w1} reaches a higher value, I_1, compare to i_{w2}, I_2. I_1 can be calculated as follows:

$$I_1 = \left[+V_{\max}a_{11} + V_{\min}a_{12} + V_{\min}\sum_{j=3}^{2n} a_{1j} \right] \times t_1, \; t_1 = x_1 \tag{8}$$

$V_{\min}$ and $V_{\max}$ are the minimum and maximum voltage of battery cells, respectively, t_1 is the duration of the first state, and $a = L^{-1}$.

The voltage variation considered around the nominal is ± 0.5 V for a 4-V battery cell. Therefore, it is not possible that the diodes D_{2U} and D_{2L} conduct since the voltage drop of diodes and the drop on the series added inductance would be

$$\begin{bmatrix} \frac{1}{L_m} + \frac{1}{L_l} + \frac{1}{L_l+L_f} & \frac{-1}{2L_l} & 0 & 0 & \dots & \frac{-1}{2L_l} \\ \frac{-1}{2L_l} & \frac{1}{L_m} + \frac{1}{L_l} & \frac{-1}{2L_l} & 0 & \dots & 0 \\ 0 & \frac{-1}{2L_l} & \frac{1}{L_m} + \frac{1}{L_l} & \frac{-1}{2L_l} & \dots & 0 \\ 0 & 0 & \frac{-1}{2L_l} & \frac{1}{L_m} + \frac{1}{L_l} & \dots & 0 \\ \dots & \dots & \dots & \dots & \dots & \dots \\ \frac{-1}{2L_l} & 0 & 0 & 0 & \frac{-1}{2L_l} & \frac{1}{L_m} + \frac{1}{L_l} \end{bmatrix}$$

$$\times \begin{bmatrix} V_1 \\ V_2 \\ V_3 \\ V_4 \\ \dots \\ V_n \end{bmatrix} = \begin{bmatrix} \frac{E_1}{L_l+L_f} \\ \frac{E_2}{L_l+L_f} \\ \frac{E_3}{L_l+L_f} \\ \frac{E_4}{L_l+L_f} \\ \dots \\ \frac{E_n}{L_l+L_f} \end{bmatrix} \rightarrow [Y_{ij}] \times [V_i] = \left[\frac{E_i}{L_l + L_f} \right] \quad 1 < i, j < n \tag{4}$$

more than 1 V. Therefore, the allowable battery voltage swing of 4 ± 0.5 V means that the MOSFET body diodes never get forward biased so as to conduct. The system inductance also contributes to prevent the diodes from conduction significant current.

The next state should be long enough to make the currents of the inductors in the first bridge reach zero. Therefore, the duration of the second state, t_2, can be calculated as follows:

$$t_2 = \frac{-I_1}{-V_{\min} a_{11} - V_{\max} a_{12} + V_{\min} \sum_{j=3}^{2n} a_{2j}}, \quad x_2 = t_1 + t_2 \,. \tag{9}$$

During the second state, the currents in bridges 2–7 ramp positively with the currents in bridges 2 and 7 reaching a higher value as they are situation closer to the bridge 1 in the circuit. Therefore, the maximum current in this state in winding 3 is

$$I_3 = \left[-V_{\min} a_{31} - V_{\max} a_{32} + V_{\min} \sum_{j=3}^{2n} a_{3j} \right] \times t_2. \tag{10}$$

The third state should be long enough to make sure all currents reach zero. Therefore, duration of this state can be calculated based on the time that takes for i_{w3} to reach zero

$$t_3 = \frac{-I_3}{-a_{3,1} V_{\min} - a_{3,2} V_{\min} - V_{\min} \sum_{j=3}^{2n} a_{3,j}},$$
$$x_3 = t_1 + t_2 + t_3. \tag{11}$$

To satisfy the design constraints that are f_s and $I_{\max}$

$$\begin{cases} T_s = T_{s,\text{desired}} \\ I_{\max} = \mathrm{I}_{\max,\text{desired}} \end{cases} \Rightarrow \begin{cases} t_1 + t_2 + t_3 = T_{s,\text{desired}} \\ I_1 = \mathrm{I}_{\max,\text{desired}} \end{cases}. \tag{12}$$

After some equation simplifications, the system design constraints can be defined as

$$A = \sum_{j=1}^{2n} a_{1j} \rightarrow$$
$$\begin{cases} t_1 + \frac{-(3V_{\min}+V_{\max})a_{13} \times [\Delta V a_{11} + V_{\min} A] \times t_1}{-V_{\min} A \times [-2V_{\min} a_{11} - (V_{\min}+V_{\max}) a_{12} + V_{\min} A]} = T_{s,\text{desired}} \\ \Delta V a_{11} + V_{\min} A \times t_1 = \mathrm{I}_{\max,\text{desired}} \end{cases}. \tag{13}$$

The unknown variables in (13) are t_1 and matrix "a" elements, these can be calculated using the magnetizing inductance of the coupled inductor and the added series inductance. It is assumed that the leakage inductance is $= 1\%$ of magnetizing inductance since the coupled inductors used normally have very low leakage inductance. As there are two equations and three unknown variables, t_1, L_m, and L_f, the series added inductance is assumed to be sized relative to the magnetizing inductance.

The design constraints for $I_{\max}$ and f_s are discussed in (12) and (13). The third constraint, maximizing the charge transfer, is satisfied by setting the duration of switching state 2 so that the first bridge currents reach zero at the end of the state. As a result, the transferred charge by other bridges and the absorbed charge by the first bridge are minimized. Since the first bridge has the highest voltage and it should be transferring charge as much as possible, the duration of state 1 is long enough so that the currents of first bridge reaches the maximum allowable current.

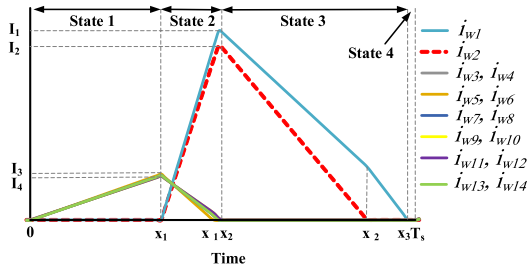

Fig. 9. Current waveforms of a seven-bridges system under case2.

This means that for state 1, the charge transfers of bridge 1 is maximized. During state 2, the other bridges are transferring charge while bridge 1 absorbs charge. The duration of state 2 is therefore minimized to limit the absorbed charge by bridge 1.

2) Extreme Case Scenario 2: Battery cell 1 has the lowest voltage, while the other battery cells have the highest voltage. Consequently, BC_1 chose the P_2 switching pattern while the rest choose P_2, see Fig. 9. The maximum bridge current in switching state 1 is

$$I_3 = \left[a_{31} V_{\min} + a_{32} V_{\max} + V_{\max} \sum_{j=3}^{2n} a_{3j} \right] \times t_1, \; x_1 = t_1. \tag{14}$$

Similar to the previous case, switching state 2 should be long enough to make sure all the currents in bridges 2–7 reach zero. Therefore, the lowest ramping rate of the currents should be considered, associated with the middle bridges as they tare least affected by bridge 1. If there are odd number of bridges, the middle bridge would be the $(n-1)/2+1$th and $(n-1)/2+2$th bridges and if the number is even, the middle bridge is the $(n-1)/2+1$th bridge: bridge 4 in a seven-bridge system. The duration of the second state is

$$t_2 = \frac{-I_4}{a_{m,1} V_{\min} + a_{m,2} V_{\max} - V_{\max} \sum_{j=3}^{2n} a_{m,j}}, x_2 = t_1 + t_2 \tag{15}$$

where the "m" subscript refers to the middle bridge. The maximum current occurs in the second inductor of the first bridge since $V_{B1} < V_{B2}$

$$I_1 = \left[+V_{\min} a_{21} + V_{\max} a_{22} - V_{\max} \sum_{j=3}^{2n} a_{1j} \right] \times t_2 \tag{16}$$

To calculate the duration of state 3, the ramping rate of i_{w1} should be considered as it has the highest current at the end of switching state 2. The third state duration should be long enough to make sure that i_{w1} returns to zero at the end of this state

$$t_3 = \frac{-I_1}{-V_{\min} a_{21} - V_{\max} a_{22} - V_{\min} \sum_{j=3}^{2n} a_{2j}},$$
$$x_3 = t_1 + t_2 + t_3. \tag{17}$$

Similar to the previous case, to get the optimum design

$$\begin{cases} T_s = T_{s,\text{desired}} \\ I_{\max} = \mathrm{I}_{\max,\text{desired}} \end{cases} \Rightarrow \begin{cases} t_1 + t_2 + t_3 = T_{s,\text{desired}} \\ I_1 = \mathrm{I}_{\max,\text{desired}} \end{cases} \tag{18}$$

After simplification, see (19) shown at the bottom of this page.

Similar to case 1, the unknown variables in (19) are t_1 and matrix "a" elements. With the same assumption, $L_l = 0.01 \times L_m$ and L_f as the same portion of L_m, t_1, and L_m for the second case can be found. After calculating all the unknown variables for the both cases, the smallest t_1, smallest t_2, and the biggest magnetizing inductance are the best design. For example, if t_1 in case 2 is bigger than t_1 in case 1, the smaller t_1 should be chosen to make sure the current does not exceed the maximum allowable value. Similarly, the magnetizing inductance is set so that current does not exceed the maximum allowable value, therefore, the bigger magnetizing inductance should be chosen.

The charge transfer occurs among all the bridges not only between adjacent bridges, this caused by the inductors being coupled. For example, in state 2, the effect of the first bridge on the other bridges is that the currents ramping rate of other bridges become higher as a negative voltage is applied to the first bridge inductors, see Fig. 4(b). The effect of other bridges on the first bridge is that the currents of first bridge return to zero faster since the other bridges have a positive voltage applied to their inductor while the first bridge has a negative voltage applied to its inductor.

C. Effect of Leakage Inductance

The effects of the leakage inductance variation on the transferred charge and charge back flow phenomenon are described.

1) Charge Transfer: Using the best design, the transferred charge in each cycle can be calculated based on the per-unit values as below

$$Q_{Bj,pu} = \frac{1}{Q_{\text{base}}}\int_0^{T_s} i_{Bj}(t)dt = \int_0^{T_s} \frac{i_{Bj}(t)}{I_{\text{base}} \times T_{\text{bases}}}dt = \int_0^{T_s} \frac{i_{Bj}(t)}{I_{\text{base}}} \times \frac{dt}{T_{\text{bases}}} = \int_0^1 i_{Bj,pu}(t_{pu}) \times dt_{pu} \tag{20}$$

where V_{base}, I_{base}, and T_{base} are the main base values, $Q_{\text{base}} = I_{\text{base}} \times T_{\text{base}}$ and $L_{\text{base}} = V_{\text{base}} \times T_{\text{base}}/I_{\text{base}}$. For example, transferred charge by battery cell 1 in a cycle in Fig. 9 is

$$\begin{aligned} Q_{B1,pu} &= \frac{1}{Q_{\text{base}}}\int_0^{T_s} i_{Bj}(t)dt \\ &= \frac{1}{Q_{\text{base}}}\left(\int_{x_1}^{x_2} i_{w1}(t)dt - \int_{x_2}^{x_2'} i_{w2}(t)dt\right) \\ &= \frac{1}{I_{\text{base}} \times T_{\text{base}}}\left(\frac{I_1 \times (x_2 - x_1)}{2} - \frac{I_2 \times (x_2' - x_2)}{2}\right) \\ &= \frac{I_{1,pu} \times (x_{2,pu} - x_{1,pu})}{2} - \frac{I_{2,pu} \times (x_{2,pu}' - x_{2,pu})}{2} \\ &\quad \times \frac{I_{1,pu} \times (t_{2,pu})}{2} - \frac{I_{2,pu} \times (t_{2,pu}')}{2} \\ &\quad \times Q_{\text{transferred}} = Q_1 + Q_2. \end{aligned} \tag{21}$$

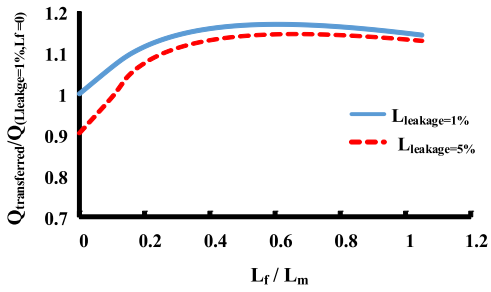

Fig. 10. Effect of series inductance on the transferred charge of a seven-bridges system $\Delta V = 5\ \%$.

The charge transferred by battery cell 1 as a function of added inductance L_f in case 1 is illustrated in Fig. 10 when the leakage is 1% and 5% for a seven-bridge system with $I_{\text{base}} = 1.5$ A, $V_{\text{base}} = 4.5$ V, $f_{s,\text{base}} = 100$ kHz, $L_m = 10\ \mu$H. The graph is normalized based on the transferred charge when there is no added inductance and leakage is 1%. As it can be observed from Fig. 10, when the value of L_f is low, the difference between transferred charge between using L_l at 1% and 5%, becomes significant but as the value of L_f increases, ΔQ is negligible, in other words, the effect of the leakage uncertainties becomes negligible as L_f dominates. The difference between charge transfer is significant, which leads to longer equalization time and more losses as the converter should operate for a longer time. As it is shown, when the series added inductance is bigger than $0.4 \times L_m$, ΔQ is negligible. Therefore, the effect of uncertainty in the leakage inductance can be mitigated by choosing the series added inductance larger than $0.4 \times L_m$. Moreover, L_f should not be chosen too high since it will slow down the transfer rate. Thus, a reasonable value is around $0.4 \times L_m$ to $0.6 \times L_m$ that should be used in the design procedure. Also, as it can be seen , when the added inductance increases from 0 to $0.5 \times L_m$ the transferred charge increases. The reason behind this phenomenon is explained in the next section.

2) Charge Back Flow: Charge back flow is a phenomenon in the third state that transfers charge from lower voltage bridges to higher voltage bridges. Although the lower series inductance is more preferable since the lower series inductance leads to lower current transfer region, shorter state 2, consequently less charge goes back to higher voltage bridges and more charge goes to lower voltage bridges, it may cause charge back flow [see Fig. 11]. The shaded area in Fig. 11 is the amount of charge that transfers back to the higher voltage bridge.

The model of a two-bridge system in the third state is shown in Fig. 12, where $V_{B1} + V_{B2} > V_{B3} + V_{B4}$. The voltage of

$$\begin{cases} t_1 + \dfrac{[a_{11}(-\Delta V + V_{\min} + 3V_{\max}) - (V_{\min} + V_{\max})A] \times [-2a_{13}\Delta V + V_{\max}A] \times t_1}{[-\Delta V a_{11} - V_{\min}A] \times [a_{1,m}(V_{\min} + 3V_{\max}) - V_{\max}A]} = T_s \\ +V_{\min}a_{21} + V_{\max}a_{22} - V_{\max}\sum_{j=3}^{2n} a_{1j} \times t_2 = \text{I}_{\text{max,desired}} \end{cases} \tag{19}$$

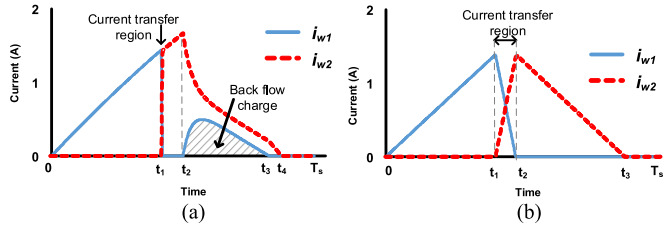

Fig. 11. Two-switch flyback for a two-bridge system: (a) low leakage and (b) high leakage.

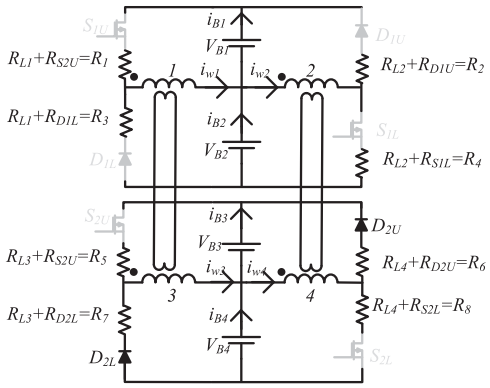

Fig. 12. Equivalent circuit of a two bridge systems when diodes of the lower voltage bridge are ON.

inductor 1 and 2 in the first bridge are

$$V_{w1} = V_{w2} = \frac{V_{w3} + V_{w4}}{L_{33} + L_{34}} \times L_{31}$$
$$V_{w3} = V_{B4} + R_7 \times i_{w3} + V_{\text{Don}}$$
$$V_{w4} = V_{B3} + R_6 \times i_{w4} + V_{\text{Don}}. \tag{22}$$

To check whether this phenomenon happens or not check the below constraints

$$\text{if} \begin{cases} V_{w2} > V_{B1} + V_{DU1} \\ \text{or} \\ V_{w1} > V_{B2} + V_{DL1} \end{cases} \tag{23}$$

The diode in bridge 1 turns ON, consequently, the current flows to charge the battery cells in bridge 1 and decrease the transferred charge to bridge 2. This problem can be prevented by increasing the series inductance, leakage, or series added inductance. It is better to increase the series added inductance since increasing the leakage inductance decreases the coupling factor between bridges. For example, in a system with $V_{\max} = 4.5$ V and $I_{\max} = 1.5$ A, the series inductance, which is enough to prevent this phenomenon, can be calculated based on, see (24) shown at the bottom of this page.

D. Design Example

The design procedure for a seven-bridge system assumes: $V_{\max} = 4.5$ V, $\Delta V = 15\%$, $I_{\max} = 1.5$ A, and $f_s = 100$ kHz is as follows.

1) Choosing L_f between $0.4 \times L_m$ and $0.6 \times L_m$.
2) Solve (13) and (19) to obtain values for L_m and t_1: all variables can be calculated for both scenarios.
3) Choose the minimum t_1 and maximum L_m from step 2.
4) Calculate t_2 based on t_1 and L_m: t_2 can be calculated based on the current constraint in case 2 ($I_2 = I_{\text{max,desired}}$).
5) For the calculated values for t_1, L_m, and t_2, check whether the desired switching frequency f_s can be used in both scenarios, if not decrease t_1 or increase L_m and go to step 3.
6) For the chosen values for t_1, L_m, t_2, and f_s, check whether the added inductance is great enough to prevent charge flow back or not, see (24). If not change the value of added inductance and go back to 2.
7) For the chosen parameters, check if the system is subject to swing or not: if yes decrease t_1 and go back to step 3.

By going through these steps, $t_1 = 38\%$, $t_2 = 15\%$, $L_m = 10$ μH, and $L_f = 4.5$ μH for this case study.

V. COMPARISON

The proposed control method is compared to a "conventional" method presented in [20]. In the conventional method, all switches are turned ON and OFF, at the same time. To understand this method, the mathematical comparison between these two methods with ideal components is done. For the conventional method, assume battery cell 1 has the highest voltage and the duration of the first state is t_1. All switches in all bridges are ON, in the first state, I_1 can be calculated as

$$I_1 = \left[V_{\max} \times a_{11} + V_{\min} \sum_{k=2}^{n} a_{1k} \right] \times t_1. \tag{25}$$

To use the whole switching cycle to transfer charge, the current should reach zero by the end of cycle. Therefore, the duration of the second state can be calculated as

$$t_2 = \frac{-I_1}{-V_{\min} \times a_{11} - V_{\max} \times a_{12} - V_{\min} \sum_{k=3}^{n} a_{jk}}. \tag{26}$$

$$\min(V_{B1}, V_{B2}) + V_{\text{Don}} > \frac{V_{B4} + V_{B3} + 2 \times V_{\text{Don}} + (R_7 \times i_{w3}) + (R_6 \times i_{w4})}{L_{33} + L_{34}} \times L_{31}$$
$$\Rightarrow \frac{\min(V_{B1}, V_{B2}) + V_{\text{Don}}}{V_{B4} + V_{B3} + 2 \times V_{\text{Don}} + (R_7 \times i_{\max}) + (R_6 \times i_{\max})} > \frac{L_{31}}{L_{33} + L_{34}}$$
$$\Rightarrow \frac{4.5 + 0.7}{9 + 2 \times 0.7 + (R_7 \times 1.5) + (R_6 \times 1.5)} = \frac{5.2}{10.4 + 1.5(R_6 + R_7)} > \frac{L_{31}}{L_{33} + L_{34}} \tag{24}$$

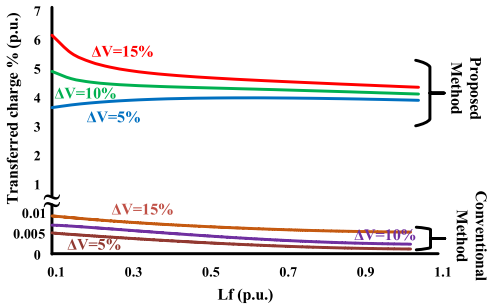

Fig. 13. Analytical prediction of transferred charge versus series added inductance under different voltage difference for both control method in ideal condition.

By applying the constraints, it can be concluded that

$$t_2 = \frac{[\Delta V \times a_{11} + V_{\min} A] \times t_1}{+\Delta V \times a_{12} + V_{\min} A}$$

$$Q_{B1} = \frac{[\Delta V \times a_{11} + V_{\min} A] \times t_1 \times t_1}{2} - \frac{[\Delta V \times a_{12} + V_{\min} A] \times t_1 \times t_2}{2} = \frac{[\Delta V \times a_{11} + V_{\min} A] \times t_1 \times t_1}{2} \times \left(1 - \frac{[\Delta V \times a_{11} + V_{\min} A]}{\Delta V \times a_{12} + V_{\min} A}\right) \quad (27)$$

The transferred charge of the conventional method can be compared with the transferred charge of the proposed method that is calculated before. While keeping the switching frequency and the maximum current similar in both methods, transferred charge by battery cell 1 in each cycle is compared for the conventional method and the proposed method, in the case when battery cell 1 has the highest voltage. To this aim, the transferred charge versus the series added inductance for bridges are illustrated in Fig. 13 for different voltage deviations in both methods. Here, $V_{\text{base}} = V_{\max} = 4.5$ V, $I_{\text{base}} = I_{\text{max,desired}} = 1.5$ A and $f_{\text{base}} = f_{s,\text{desired}} = 100$ kHz are assumed. Under these base values, $Q_{\text{base}} = I_{\text{base}} \times T_{\text{base}}$ and $L_{\text{base}} = V_{\text{base}} \times T_{\text{base}}/I_{\text{base}}$. From the graph and equations, it can be seen that ΔV and the series added inductance does not affect transferred charge in the conventional method while, as ΔV increases, the transferred charge would be higher in the proposed method. As a result, in the proposed method, at first when the voltage difference between bridges is high, the charge transfer is faster, which is advantageous.

Since equations are derived in the ideal conditions, the simulations are done with ideal and nonideal components to compare the transferred charge in the both condition. Assuming nonideal components, the interbridge charge transfer occurs at a very low rate as it is shown in Fig. 14(b) also, compare Fig. 15(a) and (b). Charge transfer in [20] is closely linked device voltage drops and the low battery cell voltage of 4 V whereas, the proposed method drastically increase the charge transfer rate as it is illustrated in Figs. 14 and 16. The equalization time is much shorter than the conventional method, with a higher power conversion

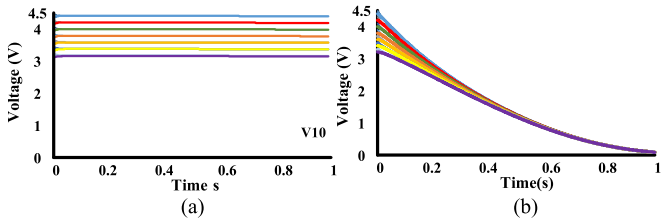

Fig. 14. Performance of a system with 14 battery cells under the method in [20] (a) without parasitic components and (b) with parasitic components.

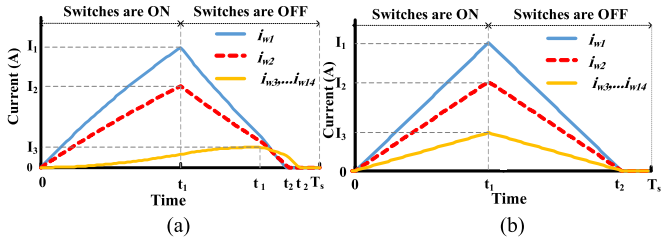

Fig. 15. Current wave form of the proposed control method (a) without parasitic components and (b) with parasitic components.

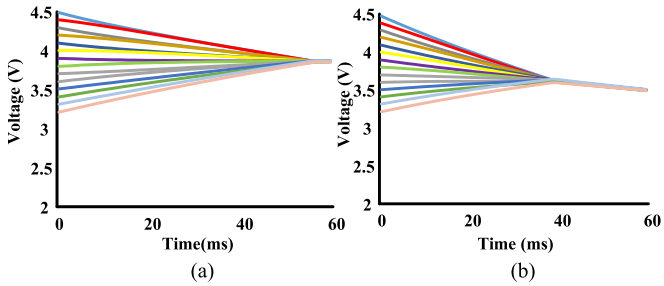

Fig. 16. Performance of a system with 14 battery cells under proposed control method in [20] (1-mF capacitors replaced actual battery cells): (a) without parasitic components and (b) with parasitic components.

efficiency. The dc voltage drop in all the BCs is high Fig. 14(b) since a 1-mF capacitor was used in the simulations to replace an actual battery cell. Simulations using larger capacitors or actual battery cell models would not produce such a large drop in the dc voltages. Here, the simulations were done with small capacitances to reach the equilibrium point faster.

VI. Simulation and Experimental Results

An experimental prototype was designed to verify the performance of the proposed controller. The system components were selected as per the design section procedure. The switching patterns for four MOSFET (20 V, 5 A) modules were obtained using a TI F28335 DSP at a switching frequency of 100 kHz, see Fig. 17. As the effect of different battery cell voltage unbalances is the main subject of investigations, four battery cells were implemented in the experimental system using three low ESR $5F$ super capacitors in parallel from SCM Series Supercapacitor. This allowed specific dc voltage unbalances to be obtained much faster than priming several battery cells at specific voltages. The four-winding transformer in each bridge was implemented using an HP2- 0216L manufactured by Coil Craft

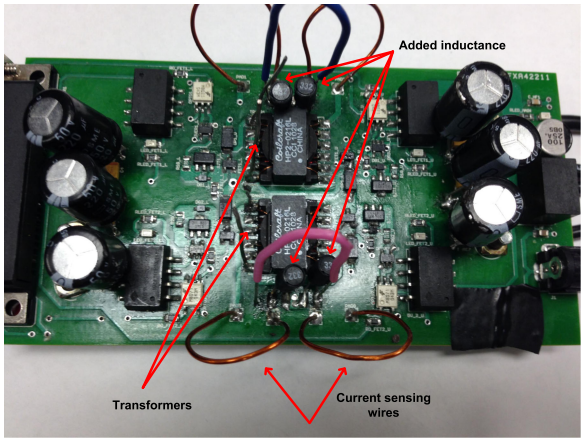

Fig. 17. Prototype of the circuit.

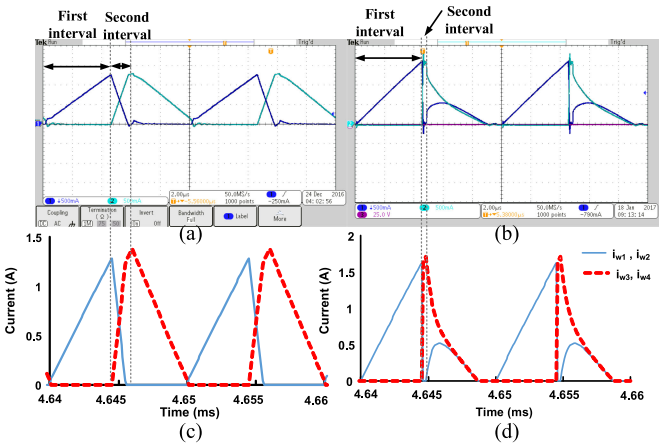

Fig. 18. Experimental results—(a) L_f added and (b) L_f removed; simulated results—(c) L_f added and (d) L_f removed.

company ($L = 10.6\ \mu$H). These transformers have six windings with windings 1 and 2 in BC as shown in Fig. 1. The coupled inductors that are used in this paper are from Coilcraft company and they are very compact, 12.9×16.3 mm. As a result, the prototype experimental circuit is also compact [see Fig. 17]. The circuit size, 60×118 mm, can comfortably fit on four battery cells. Also, it is possible for this circuit design to handle higher power and current. The main design changes would be the size of the coupled inductors, while the other components, such as switches and diodes would not be subject to significant changes in size.

A. Experimental With Designed Parameters

To verify the design procedure and parameters, which are calculated in the design section, the prototype is built with the calculated parameters. The toroidal transformers have a low leakage inductance and a series added inductance was implemented by inserting two 4.5 μH inductors into the centre-tap of the dc supply in each BC, see Figs. 1 and 17.

The experimental results of BC windings currents in Fig. 18 are close to simulations results and they match the design requirements. As it is shown in Fig. 18(a), the maximum current

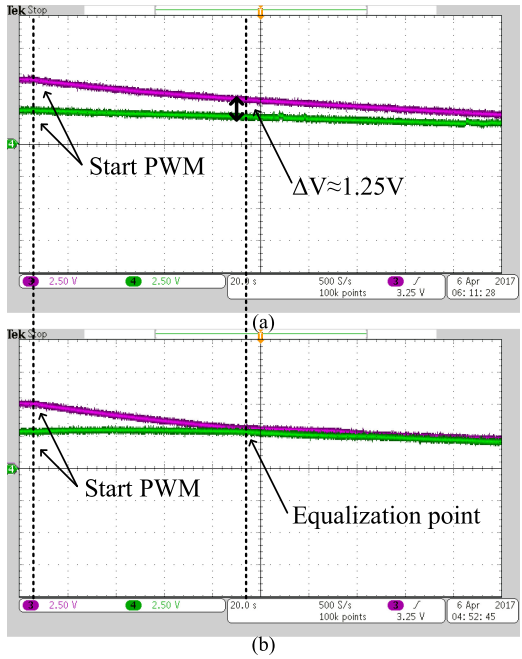

Fig. 19. Performance of the system with four 15-F capacitors under the (a) presented method in [20] and (b) proposed method.

is less than 1.5 A; switching state 2 is long enough to make sure the current of the bridge returns to zero; currents flow during the entire switching cycle.

B. Leakage Inductance Effect

The effect of adding or having no added series added inductance, L_f can be observed in Fig. 18. As the toroidal transformer has a low leakage inductance (about 1%), the low leakage situation can be tested. The duration of the state 1 period is unchanged, on-time of the BC_1 switches, but the duration of state 2 period, the on time of switches in the second bridge, is much smaller when L_f is removed. The shorter the period for state 2, the less charge is returned to the dc supply of BC_1 during this state: less charge is also removed from the dc supply of BC_2 and more charge is transferred to BC_2 from BC_1. Therefore, the average current transferring charge from BC_1 to BC_2 is better than the case of a large effective series inductance as seen in Fig. 18.

C. Performance Comparison Using Different Controllers

To study the speed of voltage equalization, two BCs were used where a battery cell was approximated using four 15-F capacitors (three 5-F capacitors connected in parallel) to replace four battery cells in a 2 BC system. The voltage of the first bridge was set to 5 V and the voltage second bridge was set to 2.5 V. For both control methods, the performance of the system is shown in Fig. 19. As it can be seen, the equalization time in the proposed method is faster than the previous method in [20]. The equalization time in the proposed method is about 100 s while in the conventional method significant voltage differences remained at 100 s. Note that for the previous method, the voltages

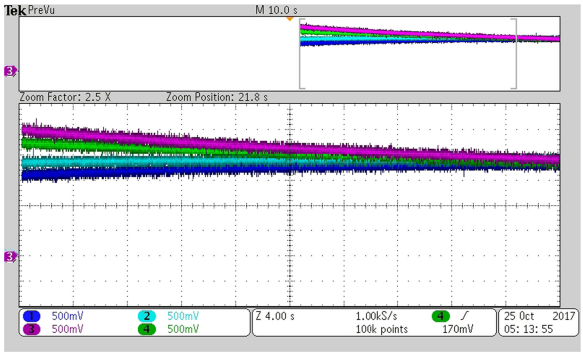

Fig. 20. Performance of the system with four 15-F capacitors under the proposed method when the voltage of batteries in a bridge are different.

of both bridges are discharging over the period shown. For the proposed method, the lower bridge voltage is maintaining its voltage, and rising slightly, while the higher voltage bridge is discharging rapidly. This means that the higher voltage bridge is transferring charge to the lower voltage bridge. This means that the rate of charge transfer is much higher than the previous method. Another experimental result is presented in Fig. 20 for the condition where the voltages of battery cells are different. In this case, the main focus is on the intrabridge charge transfer and the voltages of each battery cells are presented while the previous experimental results are focused on the interbridge charge transfer since the voltages are bridges are presented.

Also, another case where the voltage of batteries in a bridge are different is tested under the proposed control method. The results shown in Fig. 20.

VII. Discussion

There are several items that are required to be discussed more.

1) *Current Limit*: The current limit is one of the constraints in the design procedure. It can be inferred that, as the number of battery cells and bridges increase, more magnetizing inductances are added to the circuit that reduces the equivalent inductance. This may lead to higher current in the circuit. This problem can be alleviated by adding an inductance that increases the equivalent series inductance. Therefore, controlling the current, eliminating the effect of leakage inductance uncertainties and preventing charge back flow are three reasons for the added inductance existence.
2) *SOC Balancing*: The proposed controller balances the voltage of battery cells not the SOC of the battery cells. When the voltages of battery cells are the same, it does not mean their SOCs are necessarily balanced. However, one of the advantages of the proposed method is that one bridge monitors its own voltage and that of two adjacent bridges: note that each each bridge contains two battery cells. Therefore, the number of voltage sensors are halved compared with the methods that need a voltage sensor per battery cell. Although the SOC estimation is more accurate, it makes the controller more complicated and it needs a higher number of feedback signals. The SOC balancing can improve the life-time of battery cells but the procedure of the SOC estimation is pretty complex and there may be some state estimation errors. Moreover, the SOC estimation method should be completely modified when the battery cell types are changed while this is not necessary in the voltage balancing methods.
3) *Charge Transfer*: The charge transfer rate decreases as the voltages of battery cells converge. Thus, at first, when the voltage difference is high, the charge transfer rate is high and it decreases as the voltages are closer. This can be solved by adding a current sensor and modify the pulse width of the controller. This solution increases the cost and complexity of the system, but it could increase the speed of equalization. Therefore, based on the compromising among the cost, complexity, and speed of equalization, this solution can be used. This solution is not discussed in this paper since it was out of scope of this paper and it is left for the future work.
4) *Parameters Change Sensitivity*: The parameters that are subject to change in this circuit are effective leakage inductance and battery cell capacitance. The battery cell capacitance does not have any effect on the balancing procedure since the control system balances the voltage of the battery cells and does not need to estimate the SOC of the battery cell. Therefore, this system is not sensitive to battery cell capacitance change. The effect of leakage inductance change is studied in the paper and it is shown that by adding enough series inductance the effect of leakage inductance uncertainties can be eliminated. These are also added to this section.

VIII. Conclusion

Analysis, design of a new control strategy for a battery cell voltage balancing circuit are presented. The modular circuit and its control strategy is relatively easy to implement and is much faster than the conventional control methods. The proposed distributed controller is also cost effective since it just uses the local data, voltage of the bridge, and its upper and lower bridges. Moreover, the number of voltage sensor is one for each pair of battery cells, which is half when compare to the other similar methods. An equivalent circuit is introduced to simplify the calculations and make the system easier to analyze. The principle of operation of the circuit topology and controller are explained based on the main circuit and also the equivalent circuit. A design procedure is presented that provides the flexibility for using the system at different voltage and current requirements and finally, the design is optimized to get the best performance out of the system. The effect of the leakage inductance on the charge transfer rate and charge flow back are described and solution are provided to avoid them. A design example is provided and simulations and experimental results are provided to validate the design procedure. Also, a prototype, which uses the best design parameters that are calculated before, is made to get the experimental validation. It is shown that the new approach provides a much faster charge transfer in each cycle and more efficient power conversion when compared with a previous method.

REFERENCES

[1] T. H. Phung, J. C. Crebier, and Y. Lembeye, "Voltage balancing converter network for series-connected battery stack," in *Proc. IECON 2012 38th Annu. Conf. IEEE Ind. Electron. Soc.*, Oct. 2012, pp. 3007–3013.

[2] C. Mi, B. Li, D. Buck, and N. Ota, "Advanced electro-thermal modeling of lithium-ion battery system for hybrid electric vehicle applications," in *Proc. 2007 IEEE Veh. Power Propulsion Conf.*, Sep. 2007, pp. 107–111.

[3] M. Broussely *et al.*, "Main aging mechanisms in li ion batteries," *J. Power Sources*, vol. 146, no. 1, pp. 90–96, 2005.

[4] B. Lindemark, "Individual cell voltage equalizers (ice) for reliable battery performance," in *Proc. 13th Int. Telecommun. Energy Conf.*, 1991, pp. 196–201.

[5] G. Hein, "Method and apparatus for balancing capacitors in a capacitor bank," U.S. Patent 7206705, Apr. 17, 2007.

[6] T. Blank, C. Lipps, W. Ott, P. Hoffmann, and M. Weber, "Influence of environmental conditions on the sensing accuracy of li-ion battery management systems with passive charge balancing," in *Proc. 2015 17th Eur. Conf. Power Electron. Appl.*, 2015, pp. 1–9.

[7] M. Shousha, T. McRae, A. Prodic, V. Marten, and J. Milios, "Design and implementation of high power density assisting step-up converter with integrated battery balancing feature," *IEEE J. Emerging Sel. Topics Power Electron.*, vol. 5, no. 3, pp. 1068–1077, Sep. 2017.

[8] Y. Ye and K. W. E. Cheng, "Modeling and analysis of series–parallel switched-capacitor voltage equalizer for battery/supercapacitor strings," *IEEE J. Emerging Sel. Topics Power Electron.*, vol. 3, no. 4, pp. 977–983, Dec. 2015.

[9] A. C. Baughman and M. Ferdowsi, "Double-tiered switched-capacitor battery charge equalization technique," *IEEE Trans. Ind. Electron.*, vol. 55, no. 6, pp. 2277–2285, Jun. 2008.

[10] M. Evzelman, M. M. U. Rehman, K. Hathaway, R. Zane, D. Costinett, and D. Maksimovic, "Active balancing system for electric vehicles with incorporated low-voltage bus," *IEEE Trans. Power Electron.*, vol. 31, no. 11, pp. 7887–7895, Nov. 2016.

[11] M. Uno and K. Tanaka, "Single-switch cell voltage equalizer using multistacked buck-boost converters operating in discontinuous conduction mode for series-connected energy storage cells," *IEEE Trans. Veh. Technol.*, vol. 60, no. 8, pp. 3635–3645, Oct. 2011.

[12] Y.-H. Hsieh, T.-J. Liang, S.-M. O. Chen, W.-Y. Horng, and Y.-Y. Chung, "A novel high-efficiency compact-size low-cost balancing method for series-connected battery applications," *IEEE Trans. Power Electron.*, vol. 28, no. 12, pp. 5927–5939, Dec. 2013.

[13] Y. Shang, C. Zhang, N. Cui, and J. M. Guerrero, "A cell-to-cell battery equalizer with zero-current switching and zero-voltage gap based on quasi-resonant lc converter and boost converter," *IEEE Trans. Power Electron.*, vol. 30, no. 7, pp. 3731–3747, Jul. 2015.

[14] Y.-S. Lee and G.-T. Cheng, "Quasi-resonant zero-current-switching bidirectional converter for battery equalization applications," *IEEE Trans. Power Electron.*, vol. 21, no. 5, pp. 1213–1224, Sep. 2006.

[15] Y. Yuanmao, K. Cheng, and Y. Yeung, "Zero-current switching switched-capacitor zero-voltage-gap automatic equalization system for series battery string," *IEEE Trans. Power Electron.*, vol. 27, no. 7, pp. 3234–3242, Jul. 2012.

[16] C. S. Moo, Y.-C. Hsieh, and I. Tsai, "Charge equalization for series-connected batteries," *IEEE Trans. Aerosp. Electron. Syst.*, vol. 39, no. 2, pp. 704–710, Apr. 2003.

[17] T.-h. Kim, N.-j. Park, R.-y. Kim, and D.-s. Hyun, "A high efficiency zero voltage-zero current transition converter for battery cell equalization," in *Proc. 2012 27th Annu. IEEE Appl. Power Electron. Conf. Expo..*, IEEE, 2012, pp. 2590–2595.

[18] P. A. Cassani and S. S. Williamson, "Design, testing, and validation of a simplified control scheme for a novel plug-in hybrid electric vehicle battery cell equalizer," *IEEE Trans. Ind. Electron.*, vol. 57, no. 12, pp. 3956–3962, Dec. 2010.

[19] T. Gottwald, Z. Ye, and T. Stuart, "Equalization of ev and hev batteries with a ramp converter," *IEEE Trans. Aerosp. Electron. Syst.*, vol. 33, no. 1, pp. 307–312, Jan. 1997.

[20] J. Ewanchuk and J. Salmon, "A modular balancing bridge for series connected voltage sources," *IEEE Trans. Power Electron.*, vol. 29, no. 9, pp. 4712–4722, Sep. 2014.

[21] Y. Shang, B. Xia, C. Zhang, N. Cui, J. Yang, and C. C. Mi, "An automatic equalizer based on forward-flyback converter for series-connected battery strings," *IEEE Trans. Ind. Electron.*, vol. 64, no. 7, pp. 5380–5391, Jul. 2017.

[22] S. Li, C. Mi, and M. Zhang, "A high efficiency low cost direct battery balancing circuit using a multi-winding transformer with reduced switch count," in *Proc. 2012 27th Annu. IEEE Appl. Power Electron. Conf. Expo.*, 2012, pp. 2128–2133.

[23] Y. Yu, R. Saasaa, and W. Eberle, "A series resonant circuit for voltage equalization of series connected energy storage devices," in *Proc. 2016 IEEE Appl. Power Electron. Conf. Expo.*, 2016, pp. 1286–1291.

[24] G. Oriti, A. L. Julian, and P. Norgaard, "Battery management system with cell equalizer for multi-cell battery packs," in *Proc. 2014 IEEE Energy Convers. Congr. Expo.*, 2014, pp. 900–905.

[25] A. Tavakoli, S. Khajehoodin, and J. Salmon, "Switching pattern of a modular voltage balancing circuit for battery cells," in *Proc. 2016 IEEE Energy Convers. Congr. Expo.*, 2016, pp. 1–8.

[26] A. Tavakoli, I. Smith, S. Khajehoodin, and J. Salmon, "Performance comparison of two controllers for a modular voltage balancing circuit," in *Proc. 2017 IEEE Appl. Power Electron. Conf. Expo*, 2017, pp. 1667–1674.

Atrin Tavakoli (S'16) received the B.Sc. Eng. degree in electrical engineering from the Isfahan University of Technology, Isfahan, Iran, in 2011, the M.Sc. degree in power electronics from Amirkabir University of Technology, Tehran, Iran, in 2014, and is currently working toward the Ph.D. degree in battery balancer circuits and power converters at the University of Alberta, Edmonton, AB, Canada.

His research interests include power electronics applications in power and renewable energy systems and battery management systems.

S. Ali Khajehoddin (S'04–M'10–SM'16) received the B.Sc. and M.Sc. degrees in electrical engineering from the Isfahan University of Technology, Isfahan, Iran, and the Ph.D. degree in electrical engineering specialized in power electronics and their applications in renewable energy systems from Queen's University, Kingston, ON, Canada, in April 2010.

After completing the Master's degree, he cofounded a start-up company, which was focused on the development and production of power analyzers and smart metering products used for smart grid applications. For his doctoral research at Queen's University, he focused on the design and implementation of compact and durable microinverters for photovoltaic grid-connected systems. Based on this research, Queen's University spun off SPARQ systems, Inc., where, as the Lead R&D Engineer, he worked toward mass-production and commercialization of microinverters from 2010 to 2013. He joined the Department of Electrical and Computer Engineering, University of Alberta, Edmonton, AB, Canada, in 2013. He joined the Department of Electrical and Computer Engineering, University of Alberta, Edmonton, AB, Canada, in 2013, where he has been an Associate Professor since 2017.

Dr. Khajehoddin is an Associate Editor for the IEEE TRANSACTIONS ON POWER ELECTRONICS, the IEEE TRANSACTIONS ON SUSTAINABLE ENERGY, and the IEEE JOURNAL OF EMERGING AND SELECTED TOPICS IN POWER ELECTRONICS.

John Salmon (S'86–M'86) received the B.Sc. Eng. degree from Imperial College London, London, U.K., in 1982, the M.Eng. degree from McGill University, Montreal, QC, Canada, in 1984, and the Ph.D. degree from Imperial College London, London, U.K., in 1987, all in electrical engineering. In 1987, he became an Assistant Professor with the Department of Electrical Engineering, University of Alberta, Edmonton, AB, Canada, where he has been a Full Professor since 1996.

His current research interests include: power converters for electric vehicles (machine-drive systems, grid interface, charging and voltage balancing of batteries); high speed generators; utility interface of wind generators; electrical energy storage including high speed flywheels and batteries; coupled inductors for utility rectifiers and machine drive systems; pulsewidth-modulated techniques.

Dr. Salmon has received three Prize Paper Awards from the IEEE Industry Applications Society: the Industrial Drives Committee in 2008 and the Industrial Power Converter Committee in 2010 and 1994.